Supplement of

Secondary ice production affects tropical convective clouds under different aerosol conditions

Mengyu Sun et al.

Correspondence to: Mengyu Sun (mengyu.sun@manchester.ac.uk)
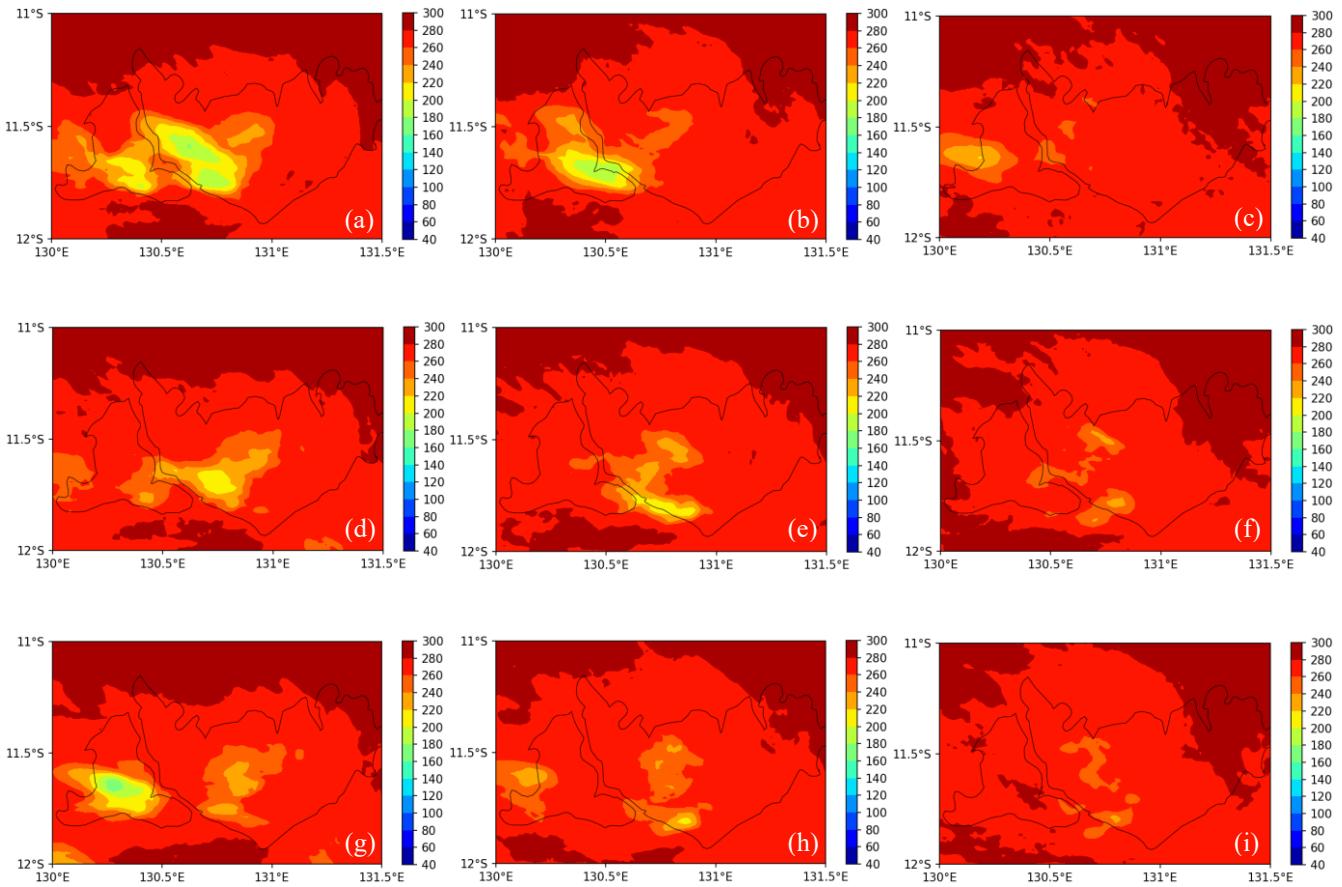
Figure S1. Spatial distribution of OLR (W m^{-2}) from noSIP simulations for (a–c) N_d = 200 cm^{-3}, (d–f) N_d = 400 cm^{-3}, and (g–i) N_d = 800 cm^{-3} at 06:30, 07:30, and 08:30 UTC on 6 February 2006.

10
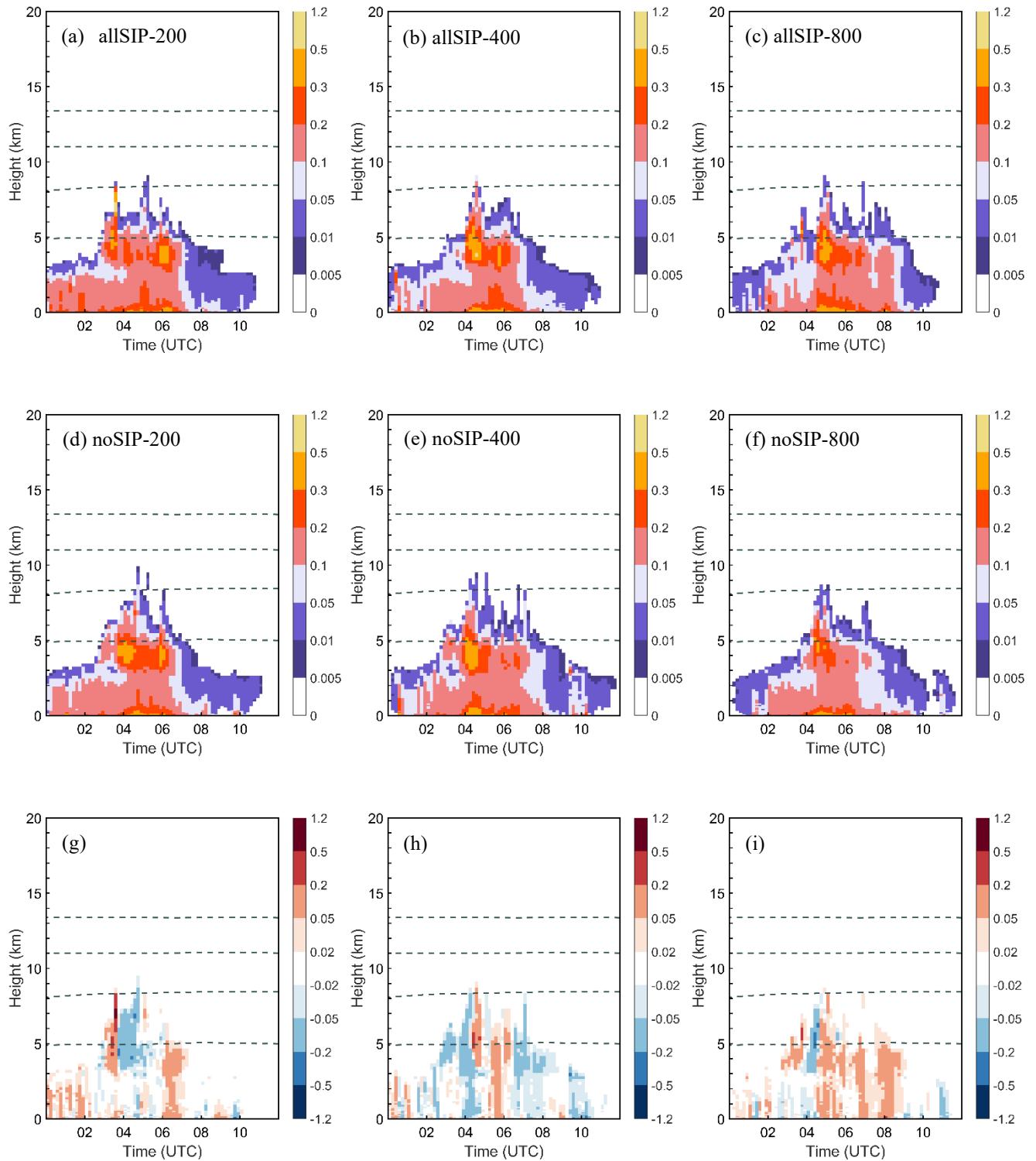
Figure S2. Time–height cross sections of rain water content (RWC; g m^{-3}) for simulations with all SIP mechanisms included: (a) allSIP-200, (b) allSIP-400, and (c) allSIP-800; and without SIP: (d) noSIP-200, (e) noSIP-400, and (f) noSIP-800. Panels (g–i) show the differences between allSIP and noSIP simulations at each CCN concentration (N_d = 200, 400, 800 cm^{-3}; i.e., allSIP minus noSIP). Panels (a–f) are averaged over the area where either the ice water path or rain water path exceeds 1 g m^{-2}. The 0, −20, −40, and −60 °C isotherms are shown by the dashed lines.
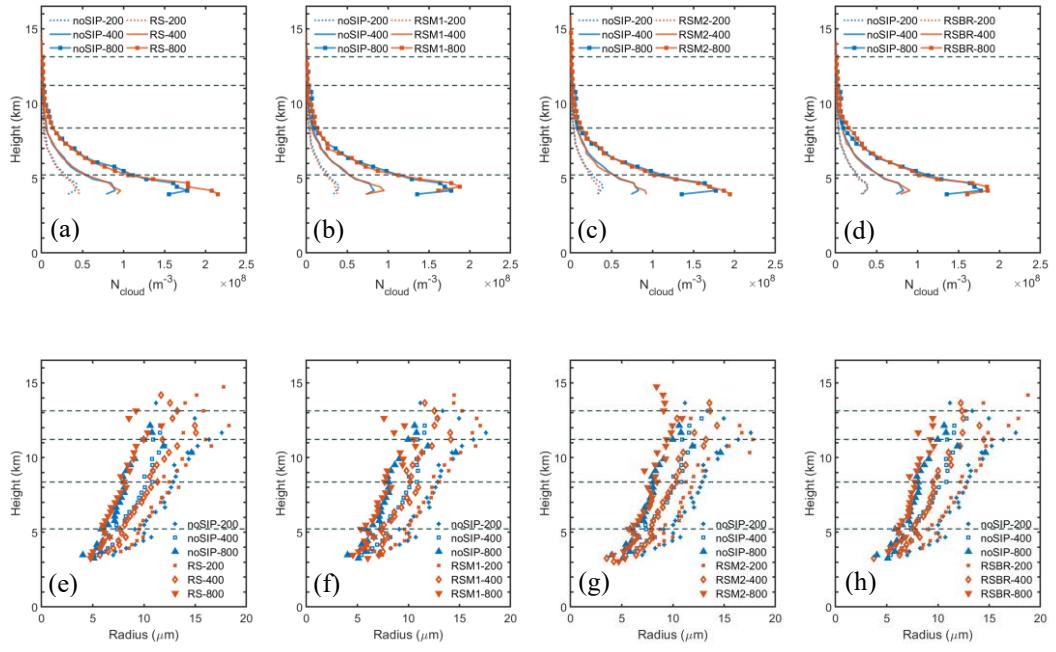
Figure S3. Vertical profiles of horizontally averaged (a-d) number concentration of cloud droplet (N_{cloud}) and (e-h) mean-mass radius of cloud droplet, from simulations without SIP (noSIP) and with different SIP configurations: (a, e) RS, (b, f) RSM1, (c, g) RSM2, and (d, h) RSBR. Dotted lines denote $N_d = 200$ cm^{-3}, solid lines denote $N_d = 400$ cm^{-3}, and solid lines with square markers denote $N_d = 800$ cm^{-3}. All profiles are averaged over the area where either the ice water path or rain water path exceeds 1 g m^{-2}, during 02:30–08:30 UTC on 6 February 2006. Gray dashed lines indicate the 0, −20, −40, and −60 °C isotherms.
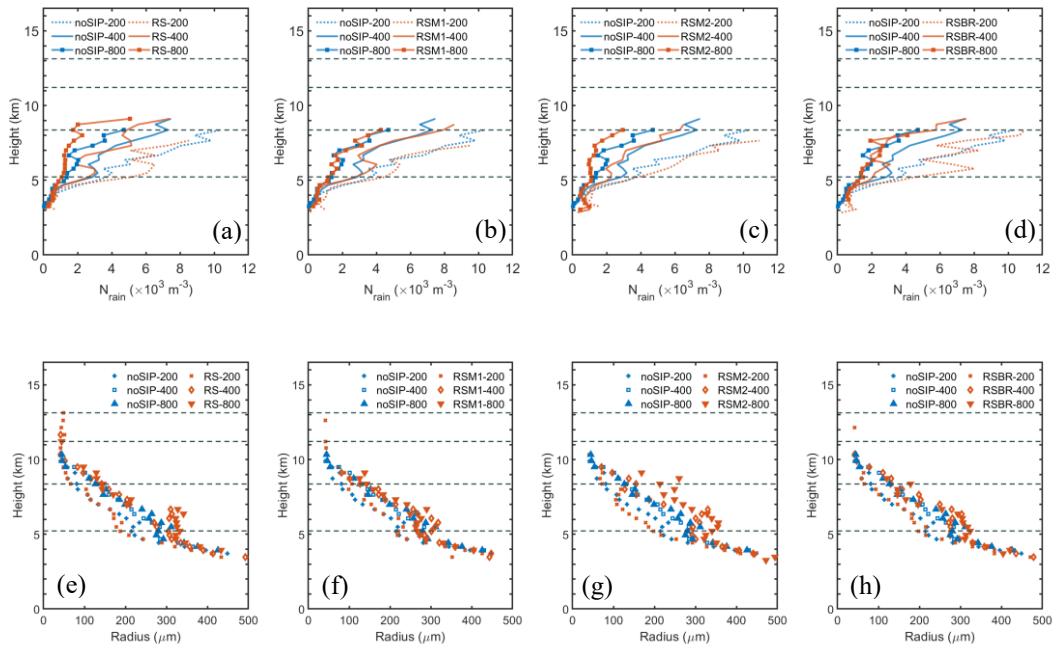
Figure S4. Same as Figure S3, but for (a-d) rain number concentration (N_{rain}), and (e-h) rain mean-mass radius.